

SUMSS: A Wide-Field Radio Imaging Survey of the Southern Sky. I. Science goals, survey design and instrumentation

(To appear in *The Astronomical Journal*)

D. C.-J. Bock¹, M. I. Large & Elaine M. Sadler

School of Physics, University of Sydney, NSW 2006, Australia

Electronic mail: dbock@astro.berkeley.edu, large@physics.usyd.edu.au, ems@physics.usyd.edu.au

ABSTRACT

The Molonglo Observatory Synthesis Telescope, operating at 843 MHz with a 5 square degree field of view, is carrying out a radio imaging survey of the sky south of declination -30° . This survey (the Sydney University Molonglo Sky Survey, or SUMSS) produces images with a resolution of $43'' \times 43'' \csc |\delta|$ and an rms noise level of $\sim 1 \text{ mJy beam}^{-1}$. SUMSS is therefore similar in sensitivity and resolution to the northern NRAO VLA Sky Survey (NVSS; Condon et al. 1998). The survey is progressing at a rate of about 1000 square degrees per year, yielding individual and statistical data for many thousands of weak radio sources. This paper describes the main characteristics of the survey, and presents sample images from the first year of observation.

Subject headings: Instrumentation: interferometers — radio continuum: galaxies — radio continuum: general — surveys

1. Introduction

The development of radio telescopes with resolution better than one minute of arc, and the increasing sophistication of astronomical image processing techniques, have made it possible to undertake large-scale, sub-arcminute surveys presenting the data not just in catalogue form, but also as images. Such high-resolution radio imaging surveys are analogous to optical Schmidt sky surveys, and can play a similarly valuable role in discovering new and interesting individual objects and studying the Universe on the largest scales. In the Northern Hemisphere, sub-arcminute radio surveys have been completed, or are well advanced, with the VLA (NVSS: Condon et al. 1998, and FIRST: Becker et al. 1995) and Westerbork (WENSS: Rengelink et al. 1997). The

¹present address: Radio Astronomy Laboratory, University of California at Berkeley, Berkeley, CA 94720, USA.

Sydney University Molonglo Sky Survey (SUMSS) described in this paper covers areas of sky not accessible to northern telescopes, and provides radio spectral index information in the regions of overlap.

The Molonglo Radio Observatory has a long history of radio survey work. The original telescope (the 408 MHz Molonglo Cross) had a resolution of $2.8'$. Between 1966 and 1978 its achievements included an imaging survey of the Galactic plane (Green 1974), acquisition of the data for the Molonglo Reference Catalogue of radio sources (MRC: Large et al. 1981, Large et al. 1991) and the discovery of 186 pulsars (Manchester et al. 1978). The 408 MHz Molonglo Cross was closed in 1978 and its east–west reflector was used in a new instrument, the Molonglo Observatory Synthesis Telescope (MOST), an imaging radio telescope operating at 843 MHz. A review of the work of the Molonglo Cross and its conversion to the MOST was given by Mills (1991) at the symposium celebrating the 25th anniversary of the Molonglo Observatory.

After more than a decade of successful observations with, and technical enhancements of, the MOST, it became clear that it would be feasible and desirable to increase the telescope’s field of view from 1 to 5 square degrees. This project, which involved the installation of hundreds of low noise preamplifiers and associated IF amplifiers and phase shifters, was completed in March 1997. The upgraded telescope now has the capacity to survey the southern sky to faint limits at a rate of ≥ 1000 square degrees per year. This survey rate, combined with the relatively low frequency of operation, good sensitivity (rms noise level ~ 1 mJy beam $^{-1}$) and stable configuration, makes the upgraded MOST a particularly powerful tool for carrying out an all-sky radio imaging survey.

In this paper we first describe (§2) the upgraded MOST, its mode of operation and some characteristics of the wide-field radio images it produces. We then explain (§3) how our new southern radio survey has been designed, and discuss (§4) some of the planned follow-up science. A second paper (Cram et al. 1998, in preparation) will discuss the data processing pipeline. Details of the closely-related MOST Galactic plane survey ($-10^\circ < b < +10^\circ$) will be published at a later date.

2. The Molonglo Observatory Synthesis Telescope

The MOST (Mills 1981; Robertson 1991) is an east–west array operating at 843 MHz. It comprises two co-linear cylindrical paraboloids (‘arms’), each 11.6 m wide and 778 m long, separated by a 15 m gap. The geometrical aperture of over 18,000 m 2 is the largest of any radio telescope in the southern hemisphere.

The MOST is essentially an array of mechanically steered antenna elements which return intermediate frequency signals to a central location for image processing. The antenna elements of the MOST are 44 contiguous 17.8 m lengths of each arm (referred to as ‘bays’). Figure 1 defines the parameters of MOST’s natural coordinate system (tilt and meridian distance). Note that the MOST resembles a conventional alt–az telescope, but with the important difference that the fixed

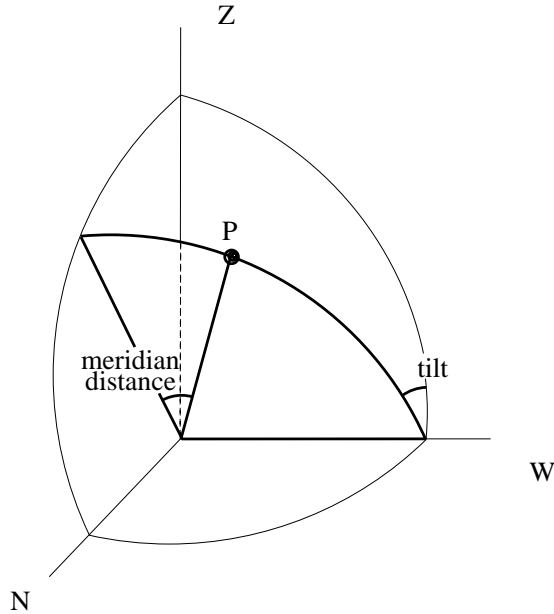


Fig. 1.— Coordinate system used with the MOST. The position, P , of a MOST beam is described by a right-handed spherical coordinate system, with the pole pointing West. *Tilt* (analogous to longitude) is measured towards North from the vertical. *Meridian distance* (analogous to latitude) is measured towards West from the meridian plane.

axis is aligned horizontally (east–west) rather than vertically. All 88 bays are steered to the same tilt by rotation of the reflectors about their east–west axis. Each bay is also steered to the same meridian distance (angular distance from the meridian plane) by differential rotation of the ring antennas (spaced at 0.54λ) which comprise the line feed.

Since the MOST is an east–west array, full aperture synthesis requires continuous observation for 12 hours. During an observation, the bays track the chosen field center, while the array tracking is achieved by introducing appropriate, frequently updated phases and delays into the signals from each bay. The meridian distance of the MOST is restricted to the range $\pm 67^\circ$. Thus, in principle, the MOST can fully synthesize in a 12-hour observation any field south of declination -23° . Fields north of -23° can be only partially synthesised. In practice, the northern declination limit for full synthesis is about -30° .

Multi-beaming circuits form a comb of 64 hard-wired real-time fan beams at the Nyquist spacing of $22''$. MOST images are formed by the technique of earth-rotation fan beam synthesis (Perley 1979; Crawford 1984). In its original configuration, the MOST had a basic field size of $23'$, extendable to $70'$ by time sharing. In preparation for the present survey (SUMSS), 352 new low-noise pre-amplifiers and associated phase shifters have been installed (Large et al. 1994). Computer control of these phase shifters enables the time-shared field size to be extended to 160 arcminutes (possibly more) by a novel technique, described in the Appendix.

Table 1 summarizes some characteristics of synthesis observations with the MOST in its wide-field mode.

2.1. Properties of the MOST wide-field images

The radio images produced by MOST differ from those produced by minimum-redundancy radio telescopes such as the VLA in three main ways:

- The uv coverage is inherently continuous, and deconvolving is a refinement rather than a necessity (see §2.1.4).
- The periodic structure of the antenna generates low-level grating ring artifacts, which may, however, be reduced by subsequent processing (see §2.2.1).
- While self-calibration is possible, it is not straightforward and requires some non-standard techniques (see §2.1.4).

Below, we describe the general properties of the MOST wide-field images used in the SUMSS, illustrated by examples from the first year of the survey.

2.1.1. Image size and resolution

As noted in Table 1, a 12-hour MOST wide-field observation centered at declination δ yields an elliptical image of dimensions $163' \times 163' \text{cosec } |\delta|$ (RA \times Dec), with a synthesised FWHM beam-size of $43'' \times 43'' \text{cosec } |\delta|$. The north-south extent of the field and the resolution in the north-south direction both vary with declination as a direct result of the foreshortening of the MOST when observations are made away from the meridian, as can be seen from Figure 2. Figure 2(a) shows a wide-field image centered at declination -80° ; the synthesised beam ($43.0'' \times 43.6''$) and the field of view ($2.73^\circ \times 2.77^\circ$) are both essentially circular. Figure 2(b) shows an image

Parameter	Value
Frequency	843 MHz
Bandwidth	3 MHz
Declination range (12 hr synthesis)	$-90^\circ \leq \delta < -30^\circ$
Maximum field size (RA \times Dec)	Elliptical, $163' \times 163' \text{cosec } \delta $
rms noise level (1σ)	$1\text{--}2 \text{ mJy beam}^{-1}$
Resolution (FWHM)	$43'' \times 43'' \text{cosec } \delta $
Polarization	Right circular (IEEE)

Table 1: Key characteristics of the MOST in its wide-field mode.

These figures presented separately in jpg format

Fig. 2.— Two SUMSS images at different declinations: (a) SUMSS Field 80 at declination -80° , (b) SUMSS Field 2411 at declination -33° . Note the N–S elongation of the northern field, and the higher noise level at the northern and southern extremes of the field.

centered at declination -33° , and here both the synthesized beam ($43.0'' \times 77.3''$) and the overall field ($2.73^\circ \times 4.91^\circ$) are extended north–south.

Less importantly, bandwidth and time–average smearing (Bridle & Schwab 1989) can broaden the synthesised beam away from the field center. The effect is small — the point–spread function is broadened by up to $0.6''$ in the direction tangential to the field center and by up to $3.3''$ in the radial direction. As a result peak flux densities may be reduced by up to 7%, but this is well–defined and can be corrected for in large–scale statistical source analyses. The integrated flux density is preserved.

2.1.2. Sensitivity

The rms noise in individual MOST images is a combination of thermal noise and source confusion from both the main beam and sidelobes of the MOST. The noise level varies with declination, position in the field, interference, weather conditions and operational status of the telescope. Figure 3 shows how the rms noise at the field center varies with declination. At declinations near -70° the rms noise at the center of a single wide–field image is typically $0.8\text{--}1\text{ mJy beam}^{-1}$.

The noise level in a MOST wide–field image varies across the field because of the complex antenna response of the MOST in the east–west and north–south directions. Examination of representative fields, confirmed by approximate theoretical analysis, shows that the noise increases with angular distance from the field center. At 1.3° from the field center the rms noise is about 20% higher than at the center, and increases more rapidly further out. This is most obvious in northern fields such as the one in Figure 2(b), because of the ‘stretched’ declination coverage. However, it is important to note that contours of constant noise level are approximately circular at all declinations.

The final SUMSS data product will be a set of $4^\circ \times 4^\circ$ mosaics, formed so as to recover uniform sensitivity and dynamic range by appropriate overlapping of the observed individual fields.

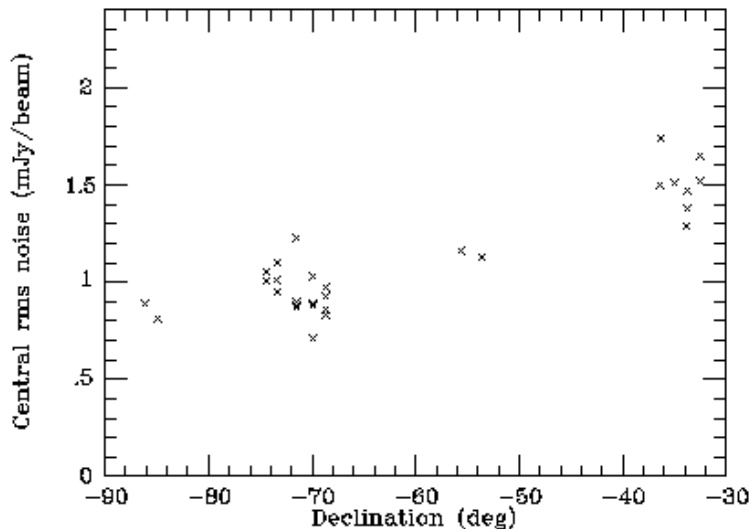


Fig. 3.— Measurements of the rms noise near the field center, for data taken in the first month of the extragalactic survey for fields well away from the Galactic plane. The noise level is higher for the northern fields, as expected.

2.1.3. Position and flux density calibration

The calibration of individual MOST images in both position and flux density is based on observations of strong calibration sources (non-variable in flux density, and of small angular size) which are made before and after each 12-hour synthesis observation². The calibrators are chosen from those listed by Campbell–Wilson & Hunstead (1994).

Typically about 5 sources are observed using a 6-minute observation known as a SCAN. Each SCAN yields three calibration factors: the ‘gain’ parameter (in Jy^{-1}), which defines the flux density scale; the ‘offset’ parameter (measured in arcseconds), which measures the mean pointing offset of the east and west arms of the telescope in the meridian distance direction; and the ‘phase’ parameter (measured in degrees), which measures the phase error between the two arms. Mean values of the SCAN parameters obtained before and after each survey are used to calibrate positions and flux densities via the Campbell–Wilson & Hunstead (1994) list of calibrators.

The flux density scale of our calibrator sources is based on the work of Hunstead (1991). It relies on an interpolation between the scales of the Molonglo Reference Catalogue (MRC) at 408 MHz (the MRC scale is very close to that of Baars et al. 1977) and the Parkes Catalogue at 2700 MHz, supplemented by absolute measurements at 843 MHz.

²The desire for complete uv coverage, and the slow slew rate of the MOST, means that calibration sources cannot be observed during a synthesis observation.

Tests on repeated fields show that for strong sources within 1° of the field center, the rms error in flux density measurement is 5% relative to our calibration sources. Within an individual field, the *relative* flux densities of unresolved strong sources can be measured with an rms error of 2% (slightly poorer near the edges of the field).

For sources weaker than about 100 mJy, thermal noise and confusion increasingly affect the accuracy of flux density measurements, contributing 1–2 mJy to the uncertainty. The final accuracy also depends on the chosen source-fitting algorithm and the dynamic range of the observations. A full discussion of these topics will be given in the second paper (Cram et al. 1998, in preparation).

The absolute and relative accuracy of flux density measurements in the final *mosaiced* images clearly depends on the calibration accuracy of the fields comprising the mosaic. This is currently $\sim 5\%$; we are investigating ways to improve the relative flux density calibration of the constituent fields in a mosaic *a posteriori*, for example by reobserving a number of fields in the same night in partial synthesis mode to tie their strongest sources together.

For strong sources within 1° of the field center, the position uncertainty is dominated by the accuracy to which the ‘offset’ and ‘phase’ parameters can be determined from each night’s SCAN calibrations. This produces typical (1σ) errors of about 1.0 arcsec in right ascension and $1.0 \times \cos \delta$ arcsec in declination.

For sources weaker than about 20 mJy the final position measurements will be limited by noise and confusion, and for resolved sources the choice of source-fitting algorithm may also affect the measured positions. Condon (1997) gives a detailed discussion of how to derive error estimates for elliptical Gaussians such as those used for radio-source fitting, and Condon et al. (1998) discuss the estimated position errors for NVSS sources as a function of flux density. We have made some simple tests which suggest that SUMSS and NVSS images have comparable positional accuracy at similar flux densities. We used the AIPS task VSAD to measure the positions and flux densities of sources in a 4.2 deg^2 region of sky near RA $22^h 43$, Dec -39° (J2000.0). We then matched the SUMSS sources with sources in the NVSS catalogue of the same region, and tabulated the position difference for each source. Within this region, there were 101 matched sources with integrated SUMSS flux densities $S_{843} > 10 \text{ mJy}$. For these sources, the mean offsets (NVSS–SUMSS) are as follows:

$$\begin{aligned}\langle \Delta \text{RA} \rangle &= -0.176 \pm 0.204 \text{ arcsec} \\ \langle \Delta \text{Dec} \rangle &= -0.129 \pm 0.314 \text{ arcsec}\end{aligned}$$

We therefore find no evidence for any significant offset between the NVSS and SUMSS reference frames. We will repeat this test with larger numbers of sources as the SUMSS survey progresses.

Figures 4(a) and (b) show the measured position differences ΔRA and ΔDec between NVSS and SUMSS positions for (a) sources with flux densities above 25 mJy, and (b) weaker sources

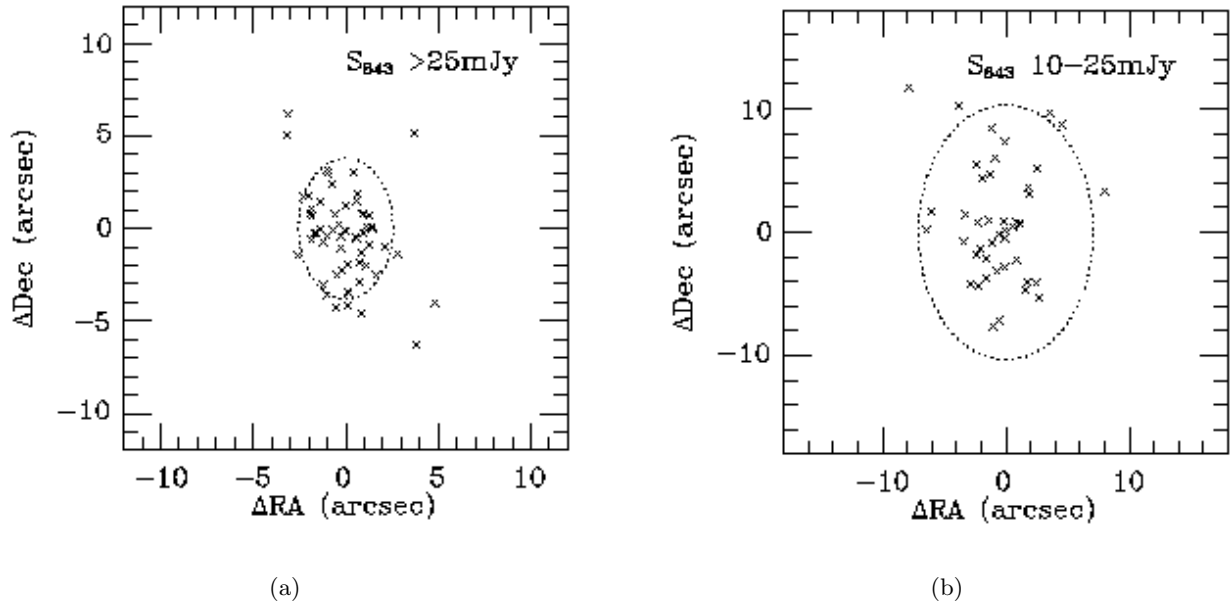


Fig. 4.— (a) Position differences in RA and Dec between SUMSS and NVSS measurements of common sources with total flux densities $S_{843} > 25 \text{ mJy}$. Dotted lines show the 90% confidence error ellipse calculated as described in the text. (b) as (a), but for weaker sources with S_{843} in the range 10–25 mJy.

with flux densities in the range 10–25 mJy. These plots are analogous to Figures 28 and 29 of Condon et al. (1998), where a similar comparison is made between positions measured by NVSS and FIRST for sources in common. Following the practice of Condon et al. (1998), we show 90% confidence ellipses constructed under the following assumptions: (i) SUMSS and NVSS position measurements of the same source have the same uncertainty in RA, while the SUMSS uncertainty in Dec is equal to the NVSS uncertainty multiplied by a factor $\text{cosec} |\delta|$ ($=1.57$ for the sources in Figure 4) to account for the stretching of the SUMSS beam in the declination direction; and (ii) the semi-axes of the 90% confidence ellipse are equal to 2.146 times the quadratic sum of the rms errors in the NVSS and SUMSS positions.

Since most of the sources in Figures 4(a) and (b) lie within the 90% confidence limits described above, our assumption that NVSS and SUMSS sources have similar position errors appears reasonable. We therefore estimate that typical SUMSS position uncertainties in RA are $\sim 5 \text{ arcsec}$ at 5 mJy, 2–3 arcsec at 10 mJy and $\sim 1 \text{ arcsec}$ above 20 mJy. Position uncertainties in declination are typically a factor $\text{cosec} |\delta|$ higher than in RA.

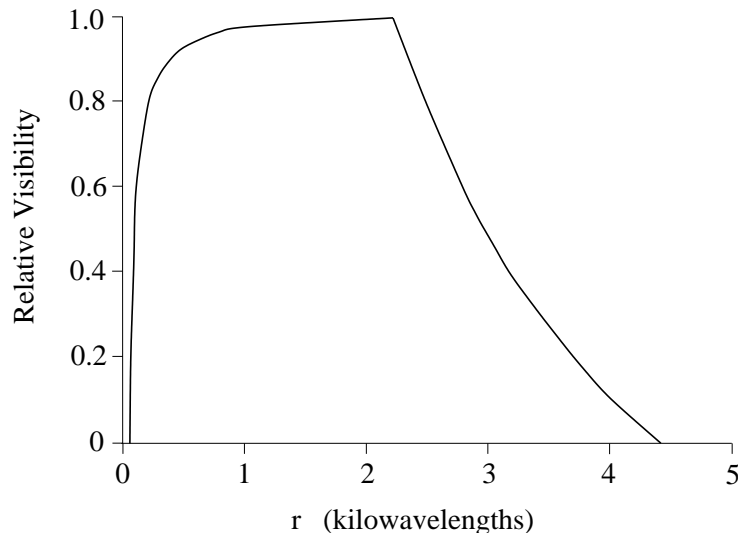


Fig. 5.— A radial profile of the effective uv weighting of the MOST’s synthesised beam (after Durdin et al. 1984)

2.1.4. *Dynamic range and the need for deconvolution*

A strength of the MOST is the continuity of uv coverage in the synthesized images. Apart from the gap due to the inter-arm spacing, all spacings are represented out to the overall length of the instrument (1570 m or 4400λ). Figure 5 shows the radial profile of the uv weighting of the MOST for a full (12-hour) synthesis. The weighting is essentially uniform from 300λ to 2500λ , then falls monotonically to zero at 4400λ .

As a result, MOST raw images look rather like conventional optical telescope images, with little need for deconvolving to make them visually acceptable or astronomically useful. This can be seen in Figure 6, which compares the CLEANed and unCLEANed image of a complex radio galaxy. SUMSS images are routinely CLEANed as part of the data reduction process, but the uniform spatial frequency coverage in the raw images means that this process is trouble-free, does not require subjective judgements to be made and does not introduce spurious features.

In raw SUMSS images, gain variations and artifacts limit the effective dynamic range (i.e. the ratio of peak source flux density to peak artifact flux density) to about 100:1. Conventional self-calibration procedures involving antenna-based corrections cannot be applied to MOST data since the signals from element pairs are not recorded individually. For fields which include one or more strong sources, an alternative technique known as ‘adaptive deconvolution’ (Cram & Ye 1995) may be used: the three telescope fan-beam parameters ‘gain’, ‘offset’ and ‘phase’ (see §2.1.3) are determined as a function of time and applied to the raw data before the image is formed. In some $70'$ fields (produced by the MOST in its original configuration), this technique has improved

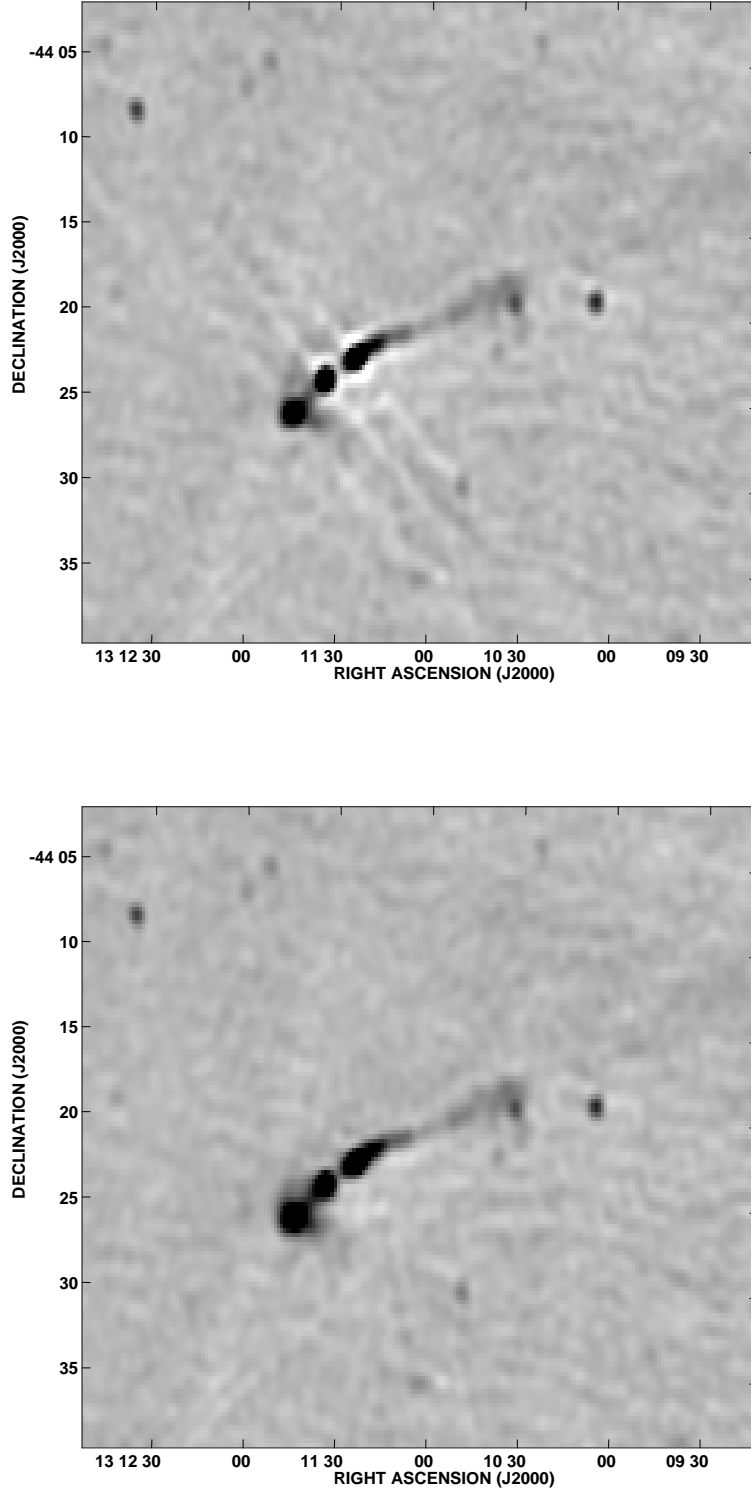


Fig. 6.— Effects of CLEAN on MOST images. These two images show the radio galaxy PKS 1308–441 before (top) and after (bottom) CLEANing. Note that that ‘dirty’ MOST maps still have good cosmetic quality, even for complex structures.

the dynamic range by a factor of ten or more. Adaptive deconvolution is used wherever possible to improve the dynamic range of SUMSS images.

2.2. Image artifacts

MOST images are affected by a number of artifacts which, having a characteristic appearance, can usually be distinguished from genuine astronomical sources. In this section we describe the effect on the image of three main sources of artifacts: sidelobes, atmospheric irregularities and interference.

2.2.1. Sidelobe response of the MOST

The only important sidelobe responses of the MOST are grating responses arising from the periodic structure of the array. In the images, the principal grating lobe appears as an ellipse of semi-diameter $4.6^\circ \times 4.6^\circ \csc |\delta|$ centered on a strong source (which may be outside the synthesized area). Although grating rings have a well-defined geometry, their amplitude is not constant around the ring: it varies with position in a field, increasing with distance from the center. Where a ring passes through the exact center of a field the amplitude is (ideally) zero. A 1 Jy unresolved source forms a grating ring with an amplitude of up to about 10 mJy beam^{-1} .

Because the amplitude of grating rings varies with distance from the field center in this way, grating rings in mosaiced images can change abruptly at the boundaries of the fields comprising the mosaic. It is often possible to remove grating rings due to known unresolved sources, though rings due to complex source structure are less tractable.

2.2.2. Atmospheric and ionospheric effects

Throughout all or part of a synthesis observation, the position of the comb of fan beams may shift irregularly. The shifts are typically ~ 1 arcsec, on a timescale of minutes. The causes of these shifts are currently under investigation; they seem to be due in part to weather-related anomalies in the distributed LO phase and in part to irregularities in ionospheric or tropospheric refraction. The effect on images is to generate a pattern of radial ‘spokes’ about sources. These features are weak, and are usually visible above the noise only for unresolved sources stronger than about 100 mJy.

Over a full 12-hour synthesis observation, the mean source displacement is zero and there is negligible effect on the determination of the flux density or source position. Self-calibration is the most effective way to reduce or eliminate the spokes.

2.2.3. *Terrestrial interference*

The operating frequency of the MOST, 843 MHz, is not in a protected radio astronomy band. However, it was chosen in consultation with Telecom Australia (now Telstra), and given some degree of local protection. In 1996–97, following joint field trials with the Australian Spectrum Management Agency (Campbell–Wilson et al. 1997), local protection of the MOST band was guaranteed until AD 2006.

The observatory has experienced short bursts of interference from ground-based transmitters, which were less frequent in 1997/98 than in previous years. Such interference is usually strong and easily recognized. Since it is short-lived and rare, the affected samples can be removed from the data before synthesis without greatly affecting the image quality. Fortunately the off-axis gain of the MOST is very low, except when an interfering source lies at the meridian distance of the main beam or its grating responses. Also, the new MOST RF and IF amplifiers have been designed to reject out-of-band interference strongly (Campbell–Wilson et al. 1997).

Radio telescopes worldwide are experiencing increasing levels of radio-frequency interference, largely as a result of the communications revolution in the last 5–10 years. MOST is not immune to RFI, but at present it does not seriously compromise our astronomical output. Despite representations to the relevant spectrum management authorities our position is not secure, and RFI is likely to become more severe in the future if usage of the band increases without agreed principles for sharing.

2.2.4. *Solar interference*

The Sun is the strongest naturally-occurring radio source in the sky, and it can cause severe interference to MOST observations made in the daytime (Campbell–Wilson et al. 1997). Consequently, observations are scheduled as far as possible at night, with the field center in transit within an hour or so of midnight. When observations overlap daylight hours we, as far as possible, plan them to minimize solar interference by avoiding daytime observations at declinations within 20° of the declination of the Sun. Solar interference appears in images as parallel bands at predictable position angles. As with other forms of interference, the effects can often be reduced to negligible levels by suitable data processing.

3. The Sydney University Molonglo Sky Survey (SUMSS) and its goals

We began the Sydney University Molonglo Sky Survey (SUMSS) in June 1997. In designing the survey, we had to take into account both our science goals and the observational constraints imposed by the MOST. Here we describe how this was done, and how we chose the survey parameters.

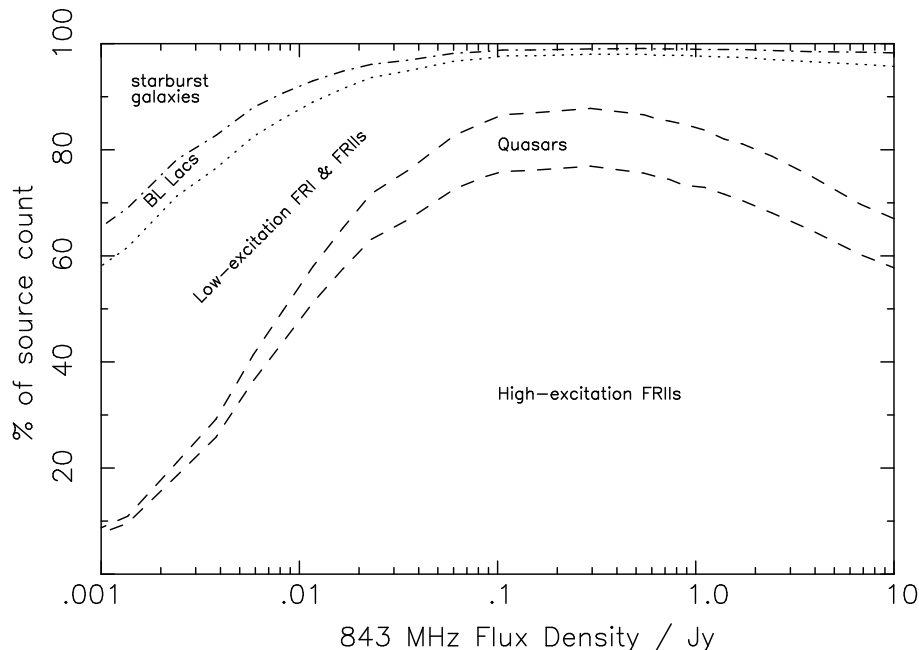


Fig. 7.— Predicted radio-source population mix at 843 MHz, from Jackson & Wall (1998).

3.1. Survey design

The design of the survey is constrained by the structure of the MOST and by our requirements for wide sky coverage, sensitivity and uniformity. The main constraints are as follows:

- Some time is needed each working day for routine maintenance of the telescope, so we can schedule, on average, nine 12-hour observations each week. As far as possible, the observing program is designed so that fields observed at night transit within an hour of midnight.
- The MOST is an east-west array with limited meridian distance coverage, and full synthesis is practicable only at declinations south of -30° as discussed in §2. Setting the northern limit of our survey at -30° therefore ensures good-quality images while giving overlap with the NVSS (Condon et al. 1998) in the declination range -30° to -40° .
- There are several reasons for aiming at a detection limit of about 5 mJy for the survey. Figure 7 shows the predicted contribution of various radio source populations as a function of flux density (Jackson & Wall 1998). It predicts that by reaching a survey limit of 5–10 mJy we will sample large numbers of both AGN and star-forming radio populations, so that both populations can be studied in detail. A 5 mJy limit also yields a high enough source density that studies of clustering and large-scale structure are possible, and is well-matched to the typical (1σ) noise level of 1.0–1.5 mJy for a single 12 h synthesis observation with the MOST.
- We want to ensure (as far as possible) uniform sensitivity across a field and from one field to

another. What can be achieved is limited by the variation of rms noise level with declination (see Figure 3) and the center-to-edge sensitivity variation of each field. The best strategy is to make individual observations on a grid of overlapped pointing centers which approximate to hexagonal close packing, then mosaic the images to recover sensitivity in the overlap regions. The NVSS (Condon et al. 1998) uses a similar strategy.

- We need to cover at least 1000 deg^2 per year to finish the survey in reasonable time, and this in turn sets limits on the amount of overlap of contiguous fields.

Each individual SUMSS field has a fully-synthesised elliptical area of $2.7^\circ \times 2.7^\circ \times (\pi/4) \times \text{cosec} |\delta|$ ($= 5.7 \text{ cosec} |\delta|$) square degrees at declination δ . In defining our survey field centers, we have assumed the ‘useful’ field to be circular with diameter 2.6° , independent of declination. This size was chosen because it corresponds to the region in which the rms noise level at the edge is no more than $\sqrt{2}$ times the value at the field center, allowing us to restore uniform sensitivity by incoherently combining the individual fields. We chose a pseudo-hexagonal close packing of field centers, using a similar scheme to that described by Condon et al. (1998) and adopted for the NVSS. (Figure 9 of the Condon et al. paper gives a useful schematic view of the field placing). As for the NVSS, our SUMSS field centers are arrayed on lines of constant declination, with a spacing such that no point on the sky is more than 1.3° from a field center. With this field spacing, the average rate of progress (i.e. area added to that already surveyed) is 4.4 square degrees per field, independent of declination

In the final grid, there are 2713 SUMSS field centers south of declination -30° . Table 2 lists the field centers and numbering convention for individual survey fields. Note that we have defined (and numbered) ‘extragalactic’ field centers for the whole sky south of declination -30° , even though we are not planning to use those within 10° of the galactic plane. Our first priority is to complete the 1118 high-latitude fields with field centers at Galactic latitude $|b| > 30^\circ$.

Table 3 compares the SUMSS survey with the three northern hemisphere radio imaging surveys now in progress or recently completed. At the time of writing (November 1998), the SUMSS survey is about 15% complete.

3.2. Data release

We intend to make the SUMSS data publicly available as the survey proceeds. The final data products will be a set of $4^\circ \times 4^\circ$ mosaiced images (using the same mosaic centers as the NVSS but extending further south) and a source catalogue. Further information (including regular updates on the progress of the survey) can be found at our survey web site, <http://www.physics.usyd.edu.au/astrop/SUMSS>.

Fields	n	Dec (J2000.0)	RA start	Δ RA	Fields	n	Dec (J2000.0)	RA start	Δ RA
1	1	–89 44 24	00 00 00	–	698–745	48	–59 56 42	00 15 00	30 m
2–7	6	–88 23 40	02 00 00	04h	746–793	48	–58 46 48	00 00 00	30 m
8–13	6	–87 23 24	00 00 00	04h	794–841	48	–57 40 48	00 15 00	30 m
14–25	12	–86 09 36	00 00 00	02h	842–889	48	–56 35 24	00 00 00	30 m
26–37	12	–84 55 12	01 00 00	02h	890–985	96	–55 34 12	00 07 30	15 m
38–49	12	–83 33 36	00 00 00	02h	986–1081	96	–53 35 24	00 00 00	15 m
50–61	12	–82 25 48	01 00 00	02h	1082–1177	96	–51 41 24	00 07 30	15 m
61–73	12	–81 20 24	00 00 00	02h	1178–1273	96	–49 53 24	00 00 00	15 m
74–97	24	–80 37 48	00 30 00	01h	1274–1369	96	–48 13 12	00 07 30	15 m
98–121	24	–79 18 00	00 00 00	01h	1370–1465	96	–46 42 36	00 00 00	15 m
122–145	24	–78 01 48	00 30 00	01h	1466–1561	96	–45 24 24	00 07 30	15 m
146–169	24	–76 45 00	00 00 00	01h	1562–1657	96	–44 06 36	00 00 00	15 m
170–193	24	–75 34 12	00 30 00	01h	1658–1753	96	–42 48 36	00 07 30	15 m
194–217	24	–74 25 12	00 00 00	01h	1754–1849	96	–41 30 36	00 00 00	15 m
218–265	48	–73 23 24	00 15 00	30 m	1850–1945	96	–40 13 12	00 07 30	15 m
266–313	48	–71 31 48	00 00 00	30 m	1946–2041	96	–38 55 48	00 00 00	15 m
314–361	48	–69 58 48	00 15 00	30 m	2042–2137	96	–37 38 24	00 07 30	15 m
362–409	48	–68 40 12	00 00 00	30 m	2138–2233	96	–36 21 00	00 00 00	15 m
410–457	48	–67 22 48	00 15 00	30 m	2234–2329	96	–35 04 12	00 07 30	15 m
458–505	48	–66 05 24	00 00 00	30 m	2330–2425	96	–33 48 00	00 00 00	15 m
506–553	48	–64 49 12	00 15 00	30 m	2426–2521	96	–32 31 12	00 07 30	15 m
554–601	48	–63 33 00	00 00 00	30 m	2522–2617	96	–31 15 36	00 00 00	15 m
602–649	48	–62 19 48	00 15 00	30 m	2618–2713	96	–29 59 24	00 07 30	15 m
650–697	48	–61 06 36	00 00 00	30 m					

Table 2: Field centres for individual SUMSS observations

	FIRST	NVSS	SUMSS	WENSS
Frequency (MHz)	1400	1400	843	325
Area (deg ²)	10,000	33,700	8,000	10,100
Resolution	5''	45''	43''	54''
Detection limit	1 mJy	2.5 mJy	5 mJy	15 mJy
Coverage	NGP	$\delta > -40^\circ$	$\delta < -30^\circ$	$\delta > +30^\circ$
Sources/deg ²	90	60	37	21

Table 3: Comparison of SUMSS with northern radio imaging surveys

This figure presented separately in jpg format

Fig. 8.— Comparison of NVSS and SUMSS mosaics for the ESO imaging survey (EIS) region.

4. Expected results of the survey

We now give a brief outline of the kinds of scientific problems which can be tackled with SUMSS data, either alone or in conjunction with data at other wavelengths.

4.1. Radio source counts

Radio source counts at 843 MHz have already been measured over areas of several square degrees by Subrahmanya and Mills (1986). They used repeated observations of several fields to improve the sensitivity, and covered a total area of 0.4 deg^2 for sources in the range 1–2 mJy, 2.3 deg^2 for sources in the range 2–7 mJy and 20 deg^2 for sources in the range 7–224 mJy. Their data were further analysed by Large (1990), who derived and tabulated integral source counts for the Subrahmanya & Mills survey area. Since Large’s original (1990) paper had very limited circulation, the integral source counts are reproduced here as Table 4.

While the SUMSS images will not go deeper than the earlier MOST source count studies, they will cover a much larger area, allowing us to compare the source counts in several areas. We would expect *a priori* to find a similar result wherever we look, but this will not be the case if the weakest sources (1–10 mJy) are clustered.

4.2. Radio spectral index measurements

The region to be observed with MOST partly overlaps the northern NVSS survey (Condon et al. 1998), which extends down to -40° declination (see Table 3). The area of overlap is 800 deg^2 . The NVSS images have similar angular resolution and sensitivity to the SUMSS (see Table 3), but are at a higher frequency (1400 MHz compared with 843 MHz).

Figure 8 shows a comparison between a 5 deg^2 SUMSS mosaic and the corresponding region from NVSS. In general the images are similar, though as noted earlier SUMSS has superior *uv* coverage and will therefore record extended emission regions with greater fidelity.

Figure 9 shows the spectral index distribution between 843 MHz and 1.4 GHz for a sample of 195 sources common to both surveys. The distribution has a median spectral index $\alpha = -0.8$ (for $S \propto \nu^{-\alpha}$). About 20% of the sources have $\alpha < -1.3$ or > -0.3 . Although care is needed in interpreting radio spectra obtained over a relatively short frequency baseline, it appears that we will be able to identify rare, but astrophysically interesting objects such as faint ultra-steep-spectrum (USS) sources which are likely to be galaxies at very high redshift (Röttgering 1993; Spinrad

S_{843} (mJy)	$N(\geq S)$	
	per steradian	per square degree
1	432,000	132
2	249 000	76
3	180 000	55
5	120 000	37
10	68 200	21
20	38 300	12
50	17 100	5.2
100	8 620	2.6
200	3 720	1.1

Table 4: Integral source counts at 843 MHz, from Large (1990)

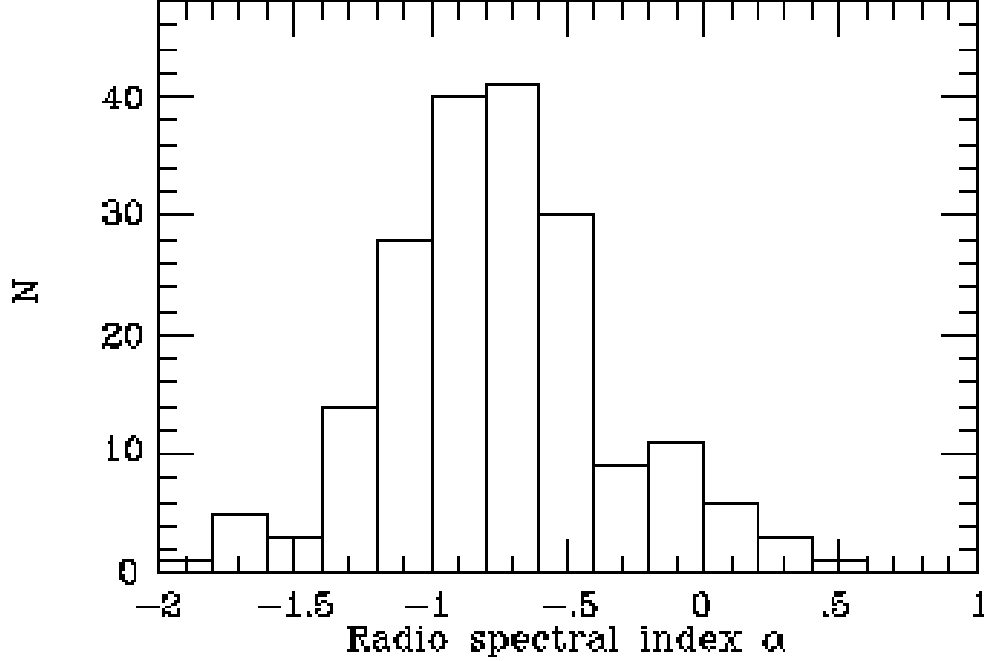


Fig. 9.— Radio spectral index distribution between 843 MHz and 1.4 GHz for 195 sources with $S_{843} > 10$ mJy observed by both NVSS and SUMSS

This figure presented separately in jpg format

Fig. 10.— 17 deg² SUMSS mosaic of a region in the southern sky. Open circles show positions of PMN sources detected at 5 GHz.

1994).

SUMSS will also yield spectral index information for several thousand strong southern radio sources through cross-identification with the PMN source catalogue (Griffith & Wright 1993), which lists sources stronger than about 50 mJy at 5 GHz. Figure 10 shows a 17 deg² region of a SUMSS mosaic of the southern sky.

Open circles mark the positions of PMN sources from an online version of the catalogue supplied by Dr Alan Wright. The higher sensitivity of the SUMSS data can clearly be seen. There are 57 PMN sources in this region, and 9 of these are clear doubles in the SUMSS images. The positional agreement with PMN is generally good, though two PMN sources have no SUMSS counterpart and another close pair of PMN sources corresponds to a single SUMSS source. Although the surface density of PMN sources is low compared to SUMSS, we expect to have about 15,000 PMN sources in our survey region. With such a large sample we can look for differences in the spectral index distribution as a function of flux density, optical identification, etc. We will also measure more accurate positions for the PMN sources, so that optical identification of the entire PMN sample can be attempted for the first time.

4.3. The two-point correlation function and source clustering

SUMSS will cover much of the southern sky to a depth of ~ 37 sources deg⁻². Such sensitivity — corresponding to a 5σ flux density limit of 5 mJy at 843 MHz — is unprecedented in the south. Earlier southern surveys had source densities of 0.5 deg⁻² for the 408 MHz Molonglo Reference Catalogue (MRC; Large et al. 1991) and 2–3 deg⁻² for the PMN 5 GHz survey (Griffith & Wright 1993).

The apparent isotropy of the radio sky reported from analysis of strong-source surveys arises mainly through sparse sampling of the source population: to detect anisotropies, a survey must reach a level faint enough for large structures to contribute more than one source to the survey. There is now convincing evidence for large-scale structure in the spatial distribution of faint radio sources (Wall et al. 1993, Kooiman et al. 1995). Cress et al. (1996) have measured the angular two-point correlation function for radio sources above 1 mJy in a 1550 square degree region of sky covered by the FIRST survey, and show that faint radio sources are clustered on scales of 0.2 to 2 degrees.

Several clustering studies are possible with SUMSS data; for example we can measure the two-point correlation function over large areas of sky, provided that our data are sufficiently

uniform in quality. The wide-field MOST images provide information on structures ~ 100 Mpc or larger, i.e. intermediate between the ~ 1 Gpc scales sampled by the COBE microwave background fluctuations and the 10–100 Mpc scales probed by optical and IRAS galaxy-clustering studies (eg. Geller & Huchra 1989; Maddox et al. 1990; Ramella et al. 1992; Benn & Wall 1995).

Without redshift measurements, however, radio-source surveys probe only the projected distribution of galaxies (radio flux densities are essentially uncorrelated with redshift, because of the broadness of the radio luminosity function). Dunlop & Peacock (1990) show that a combination of source counts with incomplete identifications and measured redshifts can be used to estimate the distribution of radio sources with redshift for different flux density limits. The first detection of the 3D clustering of radio sources was made by Peacock & Nicholson (1991), based on a redshift survey of 329 galaxies with $0.01 < z < 0.1$ and a 1400 MHz flux density above 500 mJy.

If we can determine the statistical properties of the redshift distribution of SUMSS sources as a function of flux density, it would be possible to study radio source clustering in three dimensions over a wide redshift range. This would be an ambitious project, requiring considerable follow-up time on optical telescopes.

4.4. Identification of SUMSS radio sources at other wavelengths

Cross-comparison with optical catalogues will allow us to determine which members of known classes of optical objects (for example nearby galaxies, or optically-selected QSOs) are detected as radio sources. Evolution in their radio properties with redshift is an important cosmological indicator and there are special statistical tools — such as survival analysis (Isobe et al. 1986) — to deal with low detection rates.

4.4.1. Optical identification from Digital Sky survey (DSS) images

The COSMOS database (Yentis et al. 1992) is a powerful tool for automatic identification of radio sources (Unewisse et al. 1993), and MOST positions are accurate enough for unambiguous identification of sources stronger than about 10 mJy, where the position errors are $\lesssim 1 - 2''$. For the faintest sources (~ 5 mJy) the error climbs to $\sim 5''$ (see §2.1.3), and tests using real data and randomly-offset radio positions suggest that the completeness and reliability of position-based optical identifications falls to about 50–60%.

Experience with current MOST images shows that 25–30% of sources above 5 mJy have an optical counterpart recorded by COSMOS (with the proviso noted above). For a 5 mJy detection limit, we therefore expect to detect at least 40 sources per field with COSMOS counterparts.

Current COSMOS data cover the blue (B_J) band, but two-colour (B,R) data from the Cambridge APM survey are expected to be available soon, and will give us a powerful way of

identifying rare classes of objects. For example, the optical counterparts of the most distant ($z > 4$) quasars are extremely red ($B-R > 3$; McMahon & Irwin 1991). It would be straightforward to produce a list of very red optical objects associated with radio sources for spectroscopic follow-up, in the expectation that many would be high-redshift radio-loud quasars.

4.4.2. Cross-identification with other catalogues

Cross-comparison with optical catalogues will allow us to determine which members of known classes of optical objects are detected as radio sources. Catalogues we plan to use include:

- The Third Reference Catalogue of Bright Galaxies (RC3; de Vaucouleurs et al. 1991). The detection rate of RC3 galaxies (mostly spirals) is $\sim 30\%$ in the few SUMSS fields for which a comparison has so far been made; further observations are required to establish better statistics. About 2000 RC3 galaxies fall within the area to be surveyed by SUMSS.
- The 2dF galaxy redshift survey (Colless 1998). The 2dF survey will measure redshifts for a complete sample of 250,000 southern galaxies brighter than B magnitude 19.5 over an area of 1700 deg^2 . About 2% of these galaxies are detected as radio sources by SUMSS and/or NVSS. By combining SUMSS data with the 2dF galaxy redshift survey results, it will be possible to measure the 843 MHz flux density or upper limit for a sample of about 75,000 ‘normal’ galaxies in the redshift range $0 \leq z \leq 0.3$.
- The Abell–Corwin–Olowin (ACO) catalogue of optically selected rich clusters of galaxies (Abell et al. 1989). The catalogue extends to a nominal redshift of 0.2, and lists hundreds of clusters south of declination -30° .
- An X-ray flux-limited sample of Abell clusters of galaxies compiled from ROSAT (Ebeling et al. 1996). This sample of very X-ray luminous clusters, which is essentially X-ray selected and not affected by optical extinction, contains dozens of clusters south of declination -30° .

4.4.3. Cross-identification with IRAS sources

An important tool for identifying star-forming galaxies *without* the need for optical spectroscopy makes use of the remarkably tight correlation between radio and far-infrared (FIR) luminosities (e.g. Wunderlich et al. 1987, Condon et al. 1991). For spiral galaxies, we find $S_{60\mu\text{m}} \sim 100 S_{843 \text{ MHz}}$, so MOST should detect nearly all galaxies above the IRAS Faint Source Catalog limit of 0.28 Jy at $60\mu\text{m}$. The surface density of star-forming galaxies detected in this way is about 1 per square degree, or 4–5 galaxies per SUMSS field.

5. Summary

The Molonglo Observatory Synthesis Telescope (MOST) has recently been upgraded to widen the field of view to 5 square degrees. This has enabled us to begin a deep radio imaging survey of the southern sky, with sensitivity and resolution similar to those attained by the northern NRAO VLA Sky Survey (NVSS). The reduced survey data will be made publicly available as the survey proceeds, and can be used to tackle a wide variety of astronomical problems.

The Molonglo Observatory Site Manager, Duncan Campbell–Wilson, and the technical staff Jeff Webb and Michael White have made invaluable contributions to the installation and commissioning of the new wide–field hardware. They, together with our recent appointees at the Observatory, John Van Beekhuizen and Nancye Westworth have continuing responsibility for the telescope maintenance and for running the SUMSS observational program. We warmly thank them for their dedication to these demanding tasks. We also thank Ralph Davison, who has been responsible for much of the design and fabrication of the new electronic components on which SUMSS depends, and Barbara Piestrynski who maintains the data archive. We gratefully acknowledge the contributions made by Fred Peterson, the Physics workshop and, last but not least, the academic staff, students and visitors who have been involved with the upgrade of the telescope for many years. The MOST is operated with the support of the Australian Research Council and the Science Foundation for Physics within the University of Sydney.

We also thank the anonymous referee for several useful comments and corrections.

REFERENCES

- Abell, G.O., Corwin, H.G. & Olowin, R.P., 1989, *ApJS*, 70, 1
- Amy, S.W. & Large, M.I., 1990, *PASA*, 8, 308
- Baars, J.W.M., Genzel, R., Pauliny–Toth, I.I.K., Witzel, A., 1977, *A&A*, 61, 99
- Becker, R.H., White, R.L & Helfand, D.J., 1995, *ApJ*, 450, 599
- Benn, C.R. & Wall, J.V., 1995, *MNRAS*, 272, 678
- Bridle, A.H. & Schwab, F.R., 1989, In *Synthesis imaging in radio astronomy*, ed. R. A. Perley, F. R. Schwab, & A. H. Bridle, ASP Conf. Series, p. 247
- Campbell–Wilson, D. & Hunstead, R.W., 1994, *PASA*, 11, 33
- Campbell–Wilson, D., Davidson, G. & Large, M.I., 1997, *PASA*, 14, 265
- Colless, M.M., 1998, in *Looking Deep in the Southern Sky*, ed. R. Morganti & W.J. Couch, Springer, in press.
- Condon, J.J., Broderick, J.J., 1991, *AJ*, 102, 1663

- Condon, J.J., 1997, *PASP*, 109, 166
- Condon, J.J., Cotton, W.D., Greisen, E.W., Yin, Q.F., Perley, R.A., Taylor & G.B., Broderick, J.J., 1998, *AJ*, 115, 1693
- Cram, L.E. & Ye, T., 1995, *Aust. J. Phys.*, 48, 113
- Crawford, D.F., 1984, In *Indirect imaging* ed. J.A. Roberts, Cambridge Univ. Press, p. 373
- Cress, C.M., Helfand, D.J., Becker, R.H., Gregg, M.D. & White, R.L., 1996, *AJ*, 473, 7
- de Vaucouleurs, G., de Vaucouleurs, A., Corwin, H.G., Buta, R.J., Paturel, G., Foqué, P., 1991, *Third Reference Catalogue of Bright Galaxies*, Springer
- Dunlop, J.S. & Peacock, J.A., 1990. *MNRAS* 247, 19
- Durbin, J.M., Large, M.L. & Little, A.G., 1984, In *Indirect imaging*, ed. J.A. Roberts, Cambridge Univ. Press, p. 75
- Ebeling, H., Voges, W., Bohringer, H., Edge, A.C., Huchra, J.P. & Briel, U.G., 1996, *MNRAS*, 281, 799
- Geller M.J., Huchra, J.P., 1989, *Science*, 246, 897
- Green, A.J., 1974, *A&AS*, 18, 267
- Griffith, M.R. & Wright, A.E., 1993, *AJ*, 105, 1666
- Hunstead, R.W., 1991, *AustJPhys*, 44, 743
- Isobe, T., Feigelson, E.D. & Nelson, P., 1986, *ApJ*, 306, 496
- Jackson, C.A. & Wall, J.V., 1998. In “Looking Deep in the Southern Sky”, ed. R. Morganti & W. Couch, Springer, in press.
- Kooiman, B.L., Burns, J.O., & Klypin, A.A., 1995, *ApJ*, 448, 500
- Large, M.I., Mills, B.Y., Little, A.G., Crawford, D.F. & Sutton, J.M., 1981, *MNRAS*, 194, 693
- Large, M.I., 1990. Molonglo Technical Report 90.003.
- Large, M.I., Cram, L.E. & Burgess, A.M., 1991, *Observatory*, 111, 72
- Large, M.I., Campbell–Wilson, D., Cram, L.E., Davison, R.G. & Robertson, J.G., 1994, *PASA*, 11, 44
- Maddox, S.J., Efstathiou, G., Sutherland, W.J., Loveday, J., 1990, *MNRAS*, 242, 43P
- Manchester, R.N., Lyne, A.G., Taylor, J.H., Durbin, J.M., Large, M.I. and Little, A.G., 1978, *MNRAS*, 185, 409
- McMahon, R.G. & Irwin, M., 1991, in *The space distribution of quasars*, ed. D. Crampton, ASP Conf. Series, p. 391.
- Mills, B.Y., 1981, *PASA*, 4, 156
- Mills, B.Y., 1991, *Aust. J. Phys.*, 44, 719

- Peacock, J.A. & Nicholson, D., 1991, MNRAS 253, 307
- Perley, R.A., 1979, AJ, 84, 1443
- Ramella, M., Geller, M.J., Huchra, J.P., 1992, ApJ, 384, 396
- Rengelink, R.B., Tang, Y., de Bruyn, A.G., Miley, G.K., Bremer, M.N. & Röttgering, H., 1997, A&AS, 124, 259.
- Robertson, J.G., 1991, Aust. J. Phys., 44, 729
- Röttgering, H., 1993, Ph.D. thesis, University of Leiden
- Spinrad, 1995. In *Galaxies in the young universe*, ed. H. Hippelein et al., Springer–Verlag, p. 95
- Subrahmanya, C.R., & Mills, B.Y., 1986, in *Observational Cosmology*, IAU Symposium 124, ed. A. Hewitt, G. Burbidge & L.Z. Fang, Reidel, p. 576
- Unewisse, A.M., Hunstead, R.W. & Piestrzynski, B., 1993, PASA, 10, 229
- Wall, J.V., Rixon, G.T. & Benn, C.R., 1993, in *Observational Cosmology*, ed. G. Chincarini et al., ASP Conf. Series, p. 576
- Wunderlich, E., Klein, U., Wielebinski, R., 1987, A&AS, 69, 487
- Yentis, D.J. et al., 1992, in *Digitised Optical Sky Surveys*, ed. H.T. MacGillivray & E.B. Thomson, Kluwer, p. 67.

APPENDIX

When the MOST was developed from the 408 MHz Mills Cross, the field size was limited by the available funding and by the configuration of the Cross. With the growing interest in exploiting beam-forming techniques in the next generation of radio telescopes (e.g. for the Square Kilometer Array), it is of interest to report here the techniques used to more than quadruple the original field of view of the instrument.

The MOST was formed by converting the east–west arm of the Mills Cross into a steerable phased array operating at 843 MHz. For this purpose the arm was divided into 88 bays, each 50λ long. The field of the MOST was essentially the “primary” beam of an individual bay. In the *tilt* direction the bay beamwidth (FWHM) was $\sim 2.3^\circ$, related to the physical width of the reflector. In the *meridian distance* (MD) direction it was 1.2° sec MD , set by the 50λ length of a bay. The bay length was thus a crucial parameter in the original design of the MOST, determining the field size and speed as an imaging telescope as well as the overall cost and complexity of the conversion.

A second funding-limited factor was the size of the correlator or multibeamer. The analog multibeaming system forms a *block* of 64 hard-wired fan beams, having a profile appropriate earth-rotation image synthesis. These beams are equally spaced at near the Nyquist interval of $22'' \text{ sec MD}$.³ The width of this block of beams limits the field size realized by the MOST (in its basic mode of operation) to $23' \times 23' \text{ cosec } |\delta| (\text{R.A.} \times \text{dec.})$. Sources lying outside this field, but within the primary beam of the bays, are partially synthesized.

In the original design of the MOST, provision was made to increase the fully synthesized field size by a time-sharing technique in which the comb of beams was offset $\pm 23' \text{ sec MD}$ from the field center in a 24 s cycle. This technique increases the field to $70' \times 70' \text{ cosec } |\delta|$, a nine-fold increase in sky area. It also results in a loss of sensitivity and the augmentation of grating-ring sidelobes.

In 1989, each bay was divided in two, doubling the number of independent antenna elements in the MOST from 88 to 176. At the same time a simple phase switching system was installed which allowed the beam of a bay to be offset in synchrony with the offset of the comb of fan beams. The result was a marked improvement in the quality of the $70' \times 70' \text{ cosec } |\delta|$ images. (Amy & Large 1990).

The success of the 1989 technique encouraged us to investigate methods for increasing the size of the fully synthesized field to make full use of the $\sim 2.3^\circ$ width of the primary beam in the tilt coordinate. An increased field size could be achieved only by increasing once more the number of independent elements in the array, enabling the formation of more independent fan beams. For practical and economic reasons we decided to increase the number of beams by extending the time-sharing principle, rather than by constructing a larger multibeamer or correlator. Four new

³The beams are interlaced in time with an $11''$ offset to simplify interpolation during data processing.

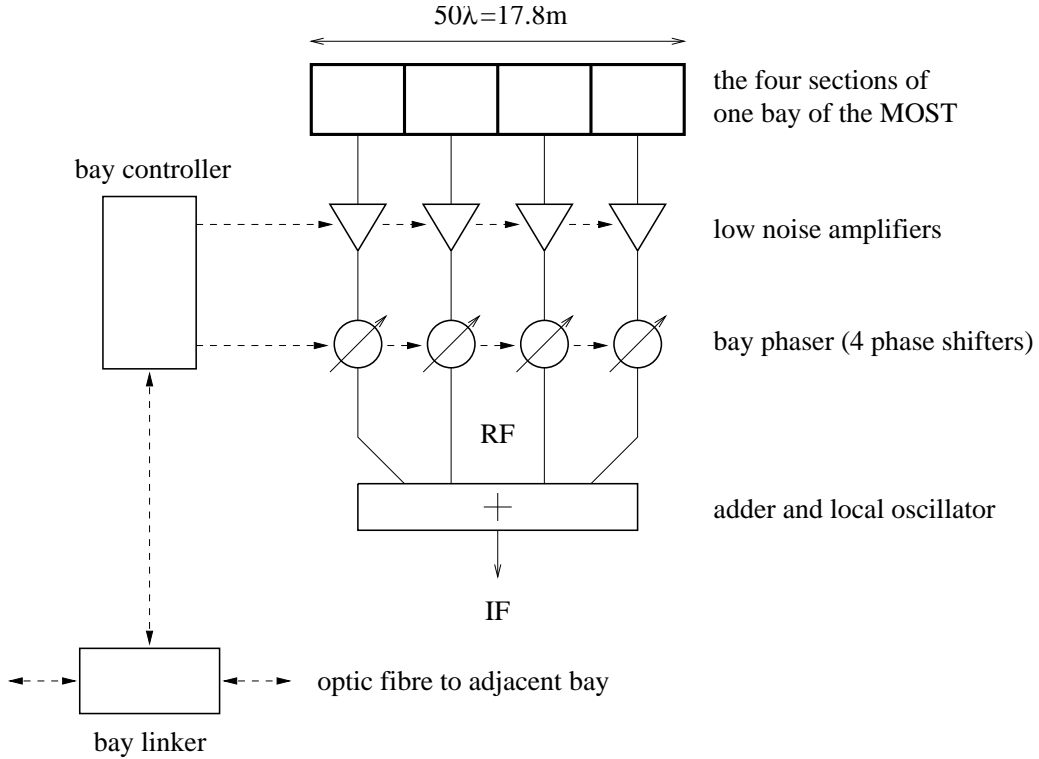


Fig. 11.— Hardware implementation of the Wide Field system. The low noise amplifiers, bay phaser, bay controller and bay linker are the components of the hardware installed at each of the 88 bays. The radio frequency (RF) and intermediate-frequency (IF) signal paths are shown as solid lines. Dashed lines indicate the control signal paths. Omitted for clarity are gain compensation circuits in the bay phaser and ancilliary control inputs and outputs on the bay controller.

low noise preamplifiers (LNA) were installed in each bay (ie one LNA for each 6.25λ length of the arm), together with computer-controlled phase shifters. The configuration is shown in Figure 11. The purpose of the phase shifters is to apply a (rapidly changeable) four-step phase gradient to the bay, thus offsetting its beam. Shifting the bay-beams in this way is analagous to the short antenna slews used in close-packed mosaicing observations with the Australia Telescope Compact array and the VLA. Electronic control of the phase shifters allows the field to be widened by cyclically offsetting the primary beam of the bays to each of N meridian distances from the nominal (tracked) field center. These offsets of the primary beam are synchronized with corresponding offsets of the comb of fan beams. The technique can be understood with reference to Figure 12. Figure 12 (a) shows the beams at meridian transit superimposed on the field (shaded circle) to be imaged by time-sharing. The grating lobes which inevitably arise from the periodic bay structure of the MOST are also shown. As can be seen in the profile, the fan beams are centered on the peak of the bay beam, while the first-order grating responses due to the bay periodicity are small as they lie at the nulls of the bay beam. Figure 12 (b) illustrates two problems which arise with

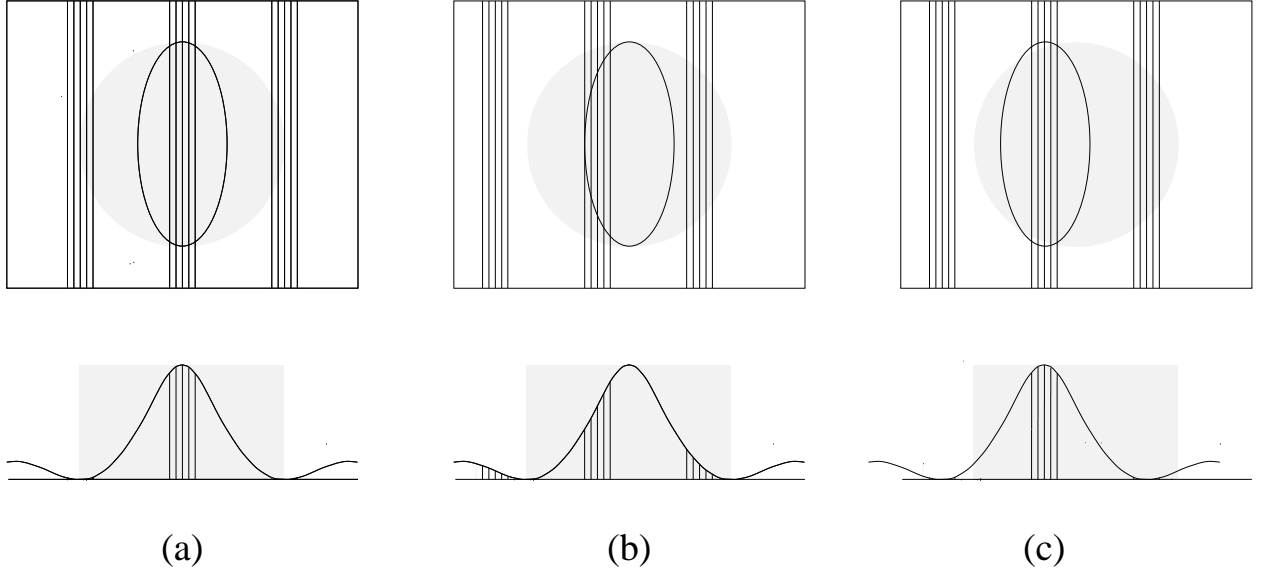


Fig. 12.— Widening the field of view of the MOST by time sharing. A representation of the MOST beams at the mid point of a 12 hour synthesis with the field to be synthesized shown as a shaded circle. In (a) the fan beams and the bay primary beam are located centrally on the field. The grating lobes (see text) are largely suppressed as they lie about the nulls of the bay primary beam, as seen in the profile. Fig. (b) shows the two problems that arise if the time-sharing is attempted by simply offsetting the fan beams: the fan beam gains are reduced and the grating responses are enhanced as they no longer lie on primary beam nulls. These problems are overcome if the primary beams are offset with the fan beams. Fig. (c) shows one of the 7 offsets used to synthesize a wide field.

the time-sharing technique when the comb of beams alone is offset:

- the gain of the principal fan beams is reduced;
- the unwanted grating responses are increased as they are shifted from the nulls of the bay beam.

Both these problems are solved by offsetting the bay beams synchronously with the fan beams, as shown in Figure 12 (c). The implementation of this facility to offset the bay beams rapidly and simultaneously with the fan beams is the essence of the upgrade which makes the survey described in this paper practicable.

Before 1997, the usual field size of MOST observations was $70' \times 70' \text{cosec } |\delta|$, the comb of beams being cycled through three positions. In the wide-field mode used for the SUMSS, the beams are (usually) cycled through 7 positions. The observing time spent on each position is thus reduced by a factor of $7/3$ and the expected signal-to-noise reduced by a factor of $\sqrt{7/3}$ (~ 1.5). The reduction in signal-to-noise has proved to be quite small, as the new preamplifiers have a markedly lower input noise. The $7/3$ increase in the meridian distance range covered by the time sharing increases the fully synthesized field area by a factor of $(7/3)^2$ (~ 5.4). In practice the increase of usable field area is somewhat less than the factor of 5.4, since the signal-to-noise deteriorates towards the extreme edge of the field as discussed in the main text.

The field area imaged by the MOST is now limited by the width of the primary (bay) beam in the tilt direction. Consequently, no further increases in the field size are possible if full synthesis of the field is to be completed in one 12 hour observation. However, in principle the data acquisition rate of the MOST could be increased by further increases in the number of independent antenna elements and fan beams. The speed of the instrument for making imaging surveys of large areas would increase pro rata, but full synthesis would depend on combining data from many days' observation.

This figure "bock.fig2a.jpg" is available in "jpg" format from:

<http://arxiv.org/ps/astro-ph/9812083v1>

This figure "bock.fig2b.jpg" is available in "jpg" format from:

<http://arxiv.org/ps/astro-ph/9812083v1>

This figure "bock.fig8.jpg" is available in "jpg" format from:

<http://arxiv.org/ps/astro-ph/9812083v1>

This figure "bock.fig10.jpg" is available in "jpg" format from:

<http://arxiv.org/ps/astro-ph/9812083v1>